PCCP

PAPER

Tuning the gallium content of metal precursors for Cu(In,Ga)Se_2 thin film solar cells by electrodeposition from a deep eutectic solvent†

Cite this: *Phys. Chem. Chem. Phys.*, 2014, **16**, 2561

João C. Malaquias,*[a] David Regesch,[b] Phillip J. Dale[a] and Marc Steichen[a]

Received 25th October 2013,
Accepted 29th November 2013

DOI: 10.1039/c3cp54509a

www.rsc.org/pccp

Controlling the Ga incorporation of Cu–In–Ga metal precursors for Cu(In,Ga)Se_2 (CIGS) solar cells is one of the main challenges for low cost electrodeposition processes, mainly due to the difficulty in electrodepositing metallic Ga from aqueous electrolytes. In this work we use the deep eutectic solvent (DES) Choline Chloride : Urea (ChCl : U – 1 : 2) to efficiently codeposit In–Ga on Cu and Mo electrodes. We control the Ga/(Ga+In) (Ga/III) ratio of the films *via* the mass fluxes. The electrochemical behavior of ChCl : U containing $GaCl_3$ and $InCl_3$ is studied by rotating disk electrode cyclic voltammetry (CV) on Mo and Cu electrodes. CV revealed on both Mo and Cu electrodes that the electrochemical behavior of the ChCl : U–$GaCl_3$–$InCl_3$ system is the superposition of the individual In and Ga electrochemistry. On a Cu electrode the morphology, crystal structure and element distribution of the deposits were a function of the Ga/III ratio. We demonstrate the precise control of Ga incorporation over a large composition range from 0.1 ≤ Ga/III ≤ 0.9 and proved that ED from DES is a straightforward, robust and efficient process. First solar cells based on Mo/Cu/In–Ga metal stacks achieved efficiencies as high as 7.9% with a V_{oc} of 520 mV.

Introduction

Cu(In,Ga)Se_2 (CIGS) is currently the best performing absorber layer material for highly efficient thin film solar cells, achieving efficiencies of up to 20.3%.[1] However, in order to make CIGS based solar cells more affordable, the production costs have to be reduced. Electrodeposition and post-annealing (EDA) is a non-vacuum process with low energy and capital cost, characterized by efficient material use and better upscaling capabilities to an industrial environment, when compared to physical vapor deposition processes. The main drawback of the EDA process is the difficulty in controlling the incorporation of Ga into the metal precursors in a facile and reproducible manner. This difficulty is due to the interfering hydrogen evolution reaction (HER), which occurs when electrodepositing gallium from aqueous solvents.

Literature, about aqueous based electrodeposition, reports on abrupt changes in the (Ga/Ga+In) (Ga/III) ratio with slight variations of the deposition potential, inability to cover the full range of this ratio (from 0.1 to 0.9), non-linear behavior of the deposit stoichiometry with metal concentration in solution, and very low plating efficiencies of around 5%.[2,3] Zank and coauthors reported on the codeposition of In–Ga on Cu from a highly toxic cyanide bath.[4] The authors were able to control the Ga/III ratio between 0 and 0.6, by tuning the deposition potential and the metal concentration in solution. The morphology of the deposits was found to be potential dependent. Electrolyte stability issues as well as homogeneity problems were encountered when depositing at very negative potentials. The authors obtained solar cells with a maximum efficiency of 6.6% over a 0.09 cm^2 surface area.

Recently, Duchatelet *et al.* codeposited Cu, In and Ga oxides with constant chemical composition *via* a complex nitrate reduction mechanism from an acid nitrate electrolyte, avoiding the HER limitation.[7,8] However, this growth route requires an additional processing phase to convert the oxide layers into metal form, which was achieved by a high temperature thermal reduction step. The authors reported a 0.1 cm^2 solar cell with 12.4% efficiency.

Another alternative to avoid the occurrence of the HER and efficiently deposit In and Ga is to use aprotic deep eutectic solvents (DES) as electroplating baths.[5,6] In this work, the DES Choline Chloride : Urea (ChCl : U – 1 : 2) is used to deposit Cu–In–Ga (with individual plating efficiencies above 85%)[5,6] in a two-step process: first copper is electrodeposited onto Mo (from ChCl : U) and then indium and gallium are co-deposited onto it.

[a] *University of Luxembourg, Laboratory for Energy Materials, 41, rue du Brill, L-4422, Belvaux, Luxembourg. E-mail: joao.malaquias@uni.lu; Fax: +352-466644-6602; Tel: +352-466644-5860*

[b] *University of Luxembourg, Laboratory for Photovoltaics, 41, rue du Brill, L-4422, Belvaux, Luxembourg*

† Electronic supplementary information (ESI) available: (1) Mathematical derivation of the relation between the mass fluxes, the Ga/III ratio and the charge passed during electrodeposition. (2) CVs of ChCl : U–$GaCl_3$–$InCl_3$ obtained from the sum of ChCl : U–$GaCl_3$ and ChCl : U–$InCl_3$ CVs on a Mo working electrode. See DOI: 10.1039/c3cp54509a

This process delivers a Cu/In–Ga metal stack with a controlled Ga/III ratio.

Under a diffusion controlled regime the Ga/III ratio, of the deposit, can be controlled *via* the ratio of the mass fluxes (J) of In and Ga – according to Fick's 1st Law. With this method we are able to finely control the Ga/III ratio over a large composition range. The mass flux is described by eqn (1):[9]

$$J = -D_0 \frac{C_0}{\delta_d}, \quad (1)$$

where D_0 is the diffusion coefficient ($cm^2\ s^{-1}$), δ_d is the diffusion layer thickness (cm) and C_0 is the concentration of the electroactive species (mol L^{-1}). The diffusion coefficient of $In^{3+/0}$ and $Ga^{3+/0}$ is 3.4×10^{-8} $cm^2\ s^{-1}$ and 8.4×10^{-8} $cm^2\ s^{-1}$, respectively at T = 60 °C.[5,6] The Ga/III ratio of the film will depend on the concentration of the metal ions in solution. The detailed mathematical description of this hypothesis can be found in the ESI.†

In this work we introduce a facile, additive free and robust method of controlling the Ga content, over a large composition range, of electrodeposited metal precursors, for CIGS solar cells, solely by tuning the metal concentration in the electrolyte.

Results and discussion

The discussion of the experimental results will be divided into three parts. The first part presents the electrochemical study of the ChCl : U–$GaCl_3$–$InCl_3$ system on a Mo electrode. The second part is centered on the electrochemistry of the same DES electrolyte on a Cu electrode. The resulting Mo/Cu/In–Ga metal stacks are characterized, focusing on their chemical composition in order to control the Ga/III ratio *via* the mass fluxes. In the third part, characterization of the CIGS absorber and the solar cell is presented.

Throughout this manuscript the composition will be described as a function of the expected Ga/III ratio of the deposit in order to maintain coherence and facilitate the connection between the different sections of the paper. To link this figure with measurable quantities and for clarity, we provide in Table 1 a correspondence between the Ga/III ratio and the used concentrations of indium ([In^{3+}]) and gallium ([Ga^{3+}]) in solution.

1. Electrochemical study of ChCl : U–$GaCl_3$–$InCl_3$ on Mo

The electrochemical behavior of ChCl : U–$GaCl_3$–$InCl_3$ on an inert Mo electrode as a function of the Ga/III ratio was studied, with the aim of investigating if alloying between In and Ga occurs.

Table 1 The expected Ga/III ratio and the corresponding concentration of In^{3+} and Ga^{3+} in solution, as expected by Fick's 1st Law

Ga/III	[In^{3+}]/mM	[Ga^{3+}]/mM
0.0	50.0	0.0
0.1	50.0	3.0
0.3	50.0	12.5
0.5	50.0	26.6
0.7	50.0	50.0
0.9	12.5	50.0
1.0	0.0	50.0

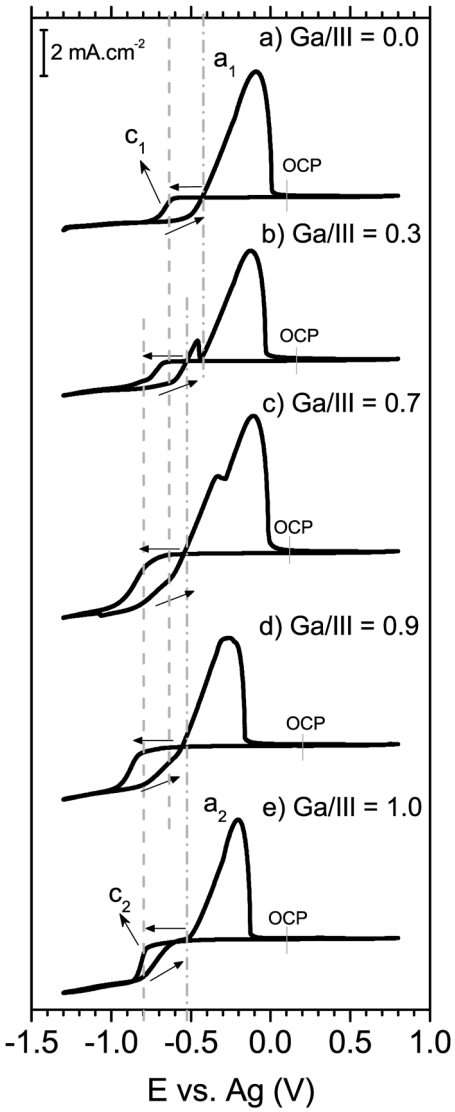

Fig. 1 RDE cyclic voltammograms of ChCl : U–$GaCl_3$–$InCl_3$ containing different concentrations of the metal chlorides on a Mo electrode. The CVs were recorded at V_{scan} = 5 mV s^{-1}, ω = 1800 rpm and T = 60 °C. The indicated Ga/III ratios are (a) 0.0, (b) 0.3, (c) 0.7, (d) 0.9 and (e) 1.0 (see Table 1).

Fig. 1 depicts a series of RDE CVs of ChCl : U–$GaCl_3$–$InCl_3$ solutions with different metal salt concentration ratios at T = 60 °C, on a Mo electrode and ω = 1800 rpm. The scanning is started at the open circuit potential (OCP) and is recorded in the negative direction. In CV (a), corresponding to a ChCl : U–$InCl_3$ solution, a cathodic current at E = −0.65 V (c_1) and an anodic peak (a_1) at E = −0.10 V are recorded. Wave c_1 corresponds to the deposition of metallic In and peak a_1 to the stripping of the indium deposited on the forward scan. Curve (e), corresponding to a ChCl : U–$GaCl_3$ solution, shows similar shape, with the deposition of Ga occurring at E = −0.80 V (wave c_2) and the stripping at E = −0.20 V (wave a_2). Nucleation loops are present in both scans as well as limiting currents over a wide potential range, indicating a diffusion controlled regime. These results are in accordance with previous observations on the Mo electrode.[5,6]

 This journal is © the Owner Societies 2014

Regarding the CVs where both metal species are present in solution – curves (b) to (d) – the reduction onset shifts from the potential of c_1 towards c_2, as the content of Ga in solution increases. The nucleation loops and limiting currents are still observed. On the reverse scan, both anodic responses a_1 and a_2 are distinguishable, particularly in scans (b) and (c). The current density of the ChCl : U–$GaCl_3$–$InCl_3$ system, particularly in the diffusion controlled regime, behaves in an additive fashion. The limiting currents in curves (c) and (d) can be obtained by the sum of the limiting currents of the individual metal salt systems in CVs (a) and (e), weighted to the corresponding Ga/III ratio. The plots demonstrating the additivity of the limiting currents are provided as ESI.† In a previous study of the ChCl : U–$CuCl_2$–$InCl_3$ system, where different Cu_xIn_y alloys were formed, such additive behavior was not observed.[6] This opposing behavior strongly indicates that there is no formation of intermetallic compounds in the system under study, in agreement with the In–Ga binary phase diagram.[10] However, an exception is observed for CV (b): the measured current density can only be obtained if the sum of (a) and (e) is weighted by a Ga/III ratio of 0.1 and not 0.3 (as expected). This particular case will be discussed in Section 2.1 of the manuscript. Tafel plot analysis[9] revealed that the exchange current on Mo for the $Ga^{3+/0}$ couple is lower than for $In^{3+/0}$ (0.13 mA cm^{-2} and 0.45 mA cm^{-2}, respectively), which indicates a faster electron transfer kinetics for the latter couple. These observations will be further discussed in Section 2.1.

The morphology of a Mo/In–Ga film, plated from a ChCl : U–$GaCl_3$–$InCl_3$ solution at T = 60 °C, ω = 300 rpm at E = −1.3 V and Ga/III = 0.4, is depicted in the SEM cross-section micrograph in Fig. 2(a), which shows the deposition of droplets with a rough surface. EDX analysis revealed the presence of In and Ga solely on the surface of the droplets. Previous work reported on the growth of smooth droplets when depositing Ga on Mo from the same electrolyte.[5] The XRD diffractogram of the referred film is presented in Fig. 2(b) and shows solely diffraction maxima related to Mo and In (JCPDS card-files 42-1120 and 05-0642, respectively). This result suggests that crystalline indium grows on the surface of gallium droplets.

To summarize, in this section we verified that the electrochemical behavior of the ChCl : U–$GaCl_3$–$InCl_3$ system on Mo was based on the superposition of the individual In and Ga systems for Ga/III > 0.3. Characterization of the deposits showed the growth of In–Ga droplets and no alloying between In and Ga on an inert Mo working electrode at 60 °C.

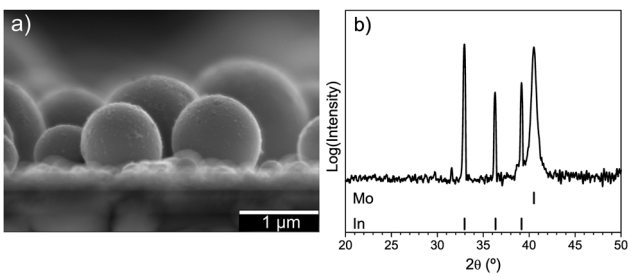

Fig. 2 (a) Cross-section SEM micrograph and (b) XRD diffractogram of a Mo/In–Ga film plated from a ChCl : U–$GaCl_3$–$InCl_3$ solution at T = 60 °C, ω = 300 rpm at E = −1.3 V.

2. Electrochemical study of ChCl : U–$GaCl_3$–$InCl_3$ on Cu

In this section the electrochemical behavior of ChCl : U–$GaCl_3$–$InCl_3$ on a Cu electrode, which is a more relevant approach when aiming for the growth of metal precursors for Cu(In,Ga)Se_2 applications, was studied. Thin films with different Ga/III ratios were electroplated onto Cu and their chemical composition is analyzed by ICP-AES to check the applicability of Fick's law under the deposition conditions. These Mo/Cu/In–Ga stacks were further characterized in terms of morphology and crystalline structure.

Fig. 3 presents RDE cyclic voltammograms of ChCl : U–$GaCl_3$–$InCl_3$ solutions with different Ga/III ratios at T = 60 °C, on a Cu electrode and at ω = 1800 rpm. Solely the potential region $E < -0.4$ V was scanned to avoid stripping the Cu electrode and contaminating the solution. In CV (a), a cathodic wave appears

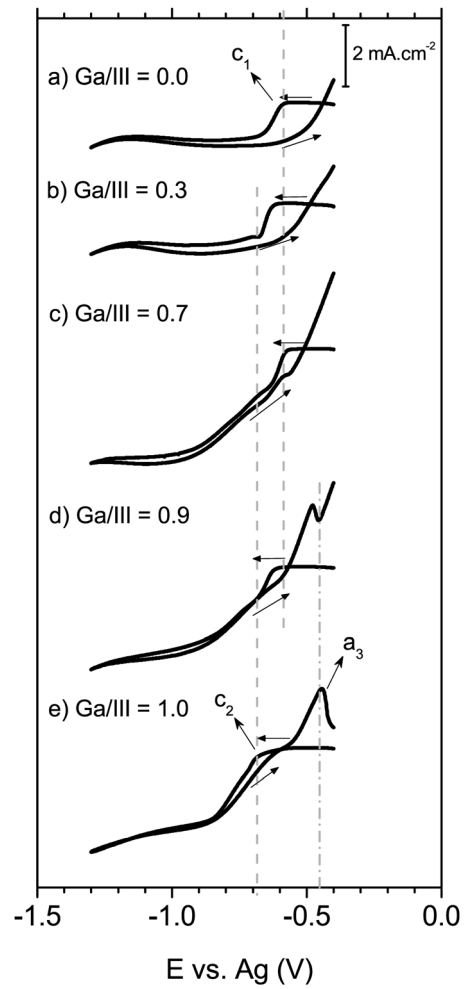

Fig. 3 RDE cyclic voltammograms of ChCl : U–$GaCl_3$–$InCl_3$ containing different concentrations of the metal chlorides on a Cu electrode. The CVs were recorded at V_{scan} = 5 mV s^{-1}, ω = 1800 rpm and T = 60 °C. The indicated Ga/III ratios are (a) 0.0, (b) 0.3, (c) 0.7, (d) 0.9 and (e) 1.0 (see Table 1).

at $E = -0.60$ V (c_1), corresponding to the deposition of indium. In scan (e), a cathodic current appears at $E = -0.70$ V (c_2), linked to Ga deposition. On the same scan, an anodic peak a_3 at $E = -0.45$ V is present and it is related to the stripping of a Cu–Ga intermetallic compound. On both scans, (a) and (e), the reduction onsets are positively shifted relative to the CVs recorded with a Mo electrode, indicating the nucleation is facilitated on Cu. Regarding the CVs with both metal species in solution – curves (b) to (d) – the reduction onset shifts from c_1 to c_2 with increasing $[Ga^{3+}]$, similar to what was discussed in Section 1 for an inert Mo electrode. The nucleation loops observed in all scans become narrower with higher Ga content in solution, showing that once the nucleation of In has started, its growth is more facile even at lower overpotentials. In CV (d) the oxidation wave a_3 is registered, indicating that during the simultaneous deposition of In and Ga, the formation of Cu_xGa_y alloys occurs. Limiting currents are observed for $E < -1.00$ V, thus the system is diffusion controlled in a 300 mV range. Similarly to the study on a Mo electrode, the limiting currents of CVs (c) and (d) are obtained by adding the single-element CVs (a) and (e), weighted to the Ga/III ratio. Analogously, curve (b) can only be fitted by considering Ga/III = 0.1. The electron transfer kinetics of $Ga^{3+/0}$ were found to be slower than $In^{3+/0}$ on a Cu electrode (0.21 mA cm^{-2} and 0.29 mA cm^{-2}, respectively), by Tafel plot analysis. An identical behavior was observed for a Mo electrode, as discussed in Section 1.

2.1 Characterization of Mo/Cu/In–Ga thin films. In order to verify if the Ga/III ratio of the deposits can be controlled using Fick's 1st Law, In and Ga were codeposited onto Mo/Cu electrodes from electrolytes with different $[Ga^{3+}]/[In^{3+}]$ ratios. The composition of the deposits was determined by ICP-AES. All depositions were carried out under rotation (ω = 300 rpm), for a constant total charge density of -0.7 C cm^{-2} and at $E = -1.2$ V to ensure time independent diffusion control.

Fig. 4(a) presents the Ga/III ratio of Mo/Cu/In–Ga analyzed by ICP-AES as a function of the expected Ga/III ratio according to Fick's Law. For each Ga/III value there are two data points plotted. The error bars on this plot arise, on one hand, from the ICP-AES measurement and, on the other hand, from the determination of the diffusion coefficient for each species and from solution preparation. Fig. 4(b)–(d) show SEM micrographs of metal stacks with Ga/III ratios ranging from 0.3 to 0.8.

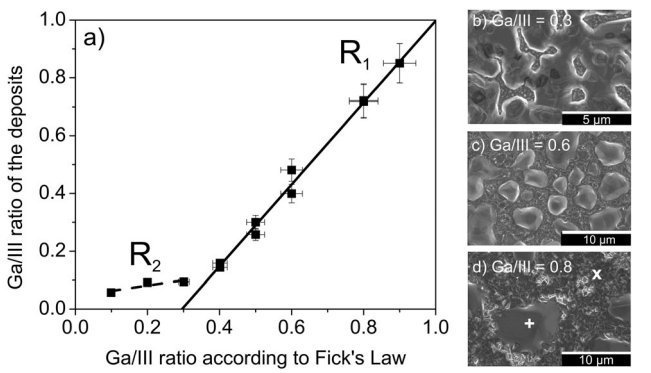

Fig. 4 Plot (a) depicts the comparison between the expected Ga/III ratio as calculated by Fick's law and those experimentally determined by ICP-AES for several Mo/Cu/In–Ga thin films. Top view SEM micrographs of metal stacks plated, with (a) Ga/III ratio of 0.3, 0.6 and 0.8, are shown in images (b), (c) and (d), respectively. The "+" and "×" in image (d) represent spots where point EDX analysis was performed.

From Fig. 4(a) it is possible to conclude that there are two different regimes: R_1 if the expected Ga/III $\geq$ 0.4 and R_2 if Ga/III $<$ 0.4. In regime R_1 the composition follows a linear trend, with the obtained Ga/III ratio ranging from 0.2 to 0.9. This regime delivers Ga/III values which are below prediction; nonetheless it follows a linear behavior as previously referred. This observation can be explained by the fact that Fick's Law only determines the number of ions that arrive at the surface of the electrode and does not account for the individual plating efficiencies. In regime R_2 the Ga/III ratio stabilizes around 0.1. This observation is related to the additivity of limited currents, discussed in Sections 1 and 2. In those sections, CV (b) in both Fig. 1 and 3 are obtained by the sum of the single element CVs (curves (a) and (e)), weighted by a Ga/III of 0.1 and not the expected 0.3, thus being in good agreement with the ICP-AES results (see ESI†). Regarding the morphology of the deposits, the micrograph in Fig. 4(b) shows a background layer with large aggregates covering a significant part of it. This film contained the lowest amount of Ga. The morphology of the films depicted in Fig. 4(c) and (d) is identical, exhibiting island growth on an underlayer. However, with increasing Ga content the average size of the islands increases from 3 µm to 8 µm and the island density decreases. Point EDX measurements were performed on the film in Fig. 4(d). The analysis revealed that the islands scattered around the surface (marked with "+" in Fig. 4(d)) are constituted by pure In, whilst the background layer (marked with "×" in the same figure) contains Cu and Ga. Additionally, both the morphology and chemical composition of the deposit are uniform across the area of the thin film. This observation can be explained by a large potential region where the mass flux is constant (*cf.* CVs in Fig. 3), which allows the process to tolerate voltage drops across the surface of the substrate. J. Zank *et al.* observed comparable morphology in thin films plated by a similar deposition route from a cyanide-based aqueous electrolyte with Ga/III of 0.14 and 0.63.[4] Kim *et al.* sputtered alternating layers of Cu–Ga and In, with an average Ga/III of 0.2 and the resulting morphology was similar to the precursor in Fig. 4(b).[11] Further electrochemical experiments showed that Ga electrodeposition occurs at more positive potentials on an In working electrode than on a Cu working electrode. These results show that the appearance of regime R_2 in Fig. 4 is not related with the observed differences in morphology, as a different In surface coverage does not influence Ga electrodeposition. To explain the appearance of R_2, we suggest that the larger radius of the indium solvated particle,[6] the slower electron transfer kinetics for the $Ga^{3+/0}$ couple and the facilitated In growth, in very indium-rich environments, hinder gallium deposition, pinning the Ga content to a maximum of Ga/III = 0.1. This effect was also observed in the cyclic voltammetry results as discussed in Sections 1 and 2, specifically in curve (b) of Fig. 1 and 3.

 This journal is © the Owner Societies 2014

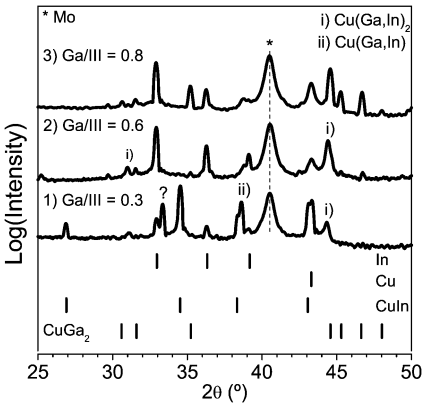

Fig. 5 XRD diffractograms of Mo/Cu/In–Ga films electrodeposited from a ChCl : U–$GaCl_3$–$InCl_3$ electrolyte at E = −1.2 V, T = 60 °C and ω = 300 rpm, with a Ga/III ratio of (1) 0.3, (2) 0.6 and (3) 0.8.

Fig. 5 presents the XRD diffractograms of the Mo/Cu/In–Ga films presented in Fig. 4(b) to (d). Metallic Cu and In (JCPDS card files 04-0836 and 05-0642, respectively) are common to all precursors. In diffractogram (1), corresponding to the film with the lowest Ga content, intense CuIn diffraction maxima (JCPDS card file 35-1150) are detected. Peaks marked with (i) and (ii) cannot be directly assigned to any JCPDS reference, however, their proximity to CuIn and $CuGa_2$ (JCPDS card file 25-0275) maxima suggests that ternary Cu(In,Ga) and $Cu(Ga,In)_2$ phases were formed. Supporting this argument are other ternary crystalline phases of $Cu_x(In,Ga)_y$ that have been reported in the literature, specifically $Cu_{11}(In,Ga)_9$, $Cu_{16}(In,Ga)_9$ and $Cu_9(In,Ga)_4$.[12–15] The peak marked with "?" in diffractogram (1) cannot be assigned to any phase existing in the JCPDS database. In diffractograms (2) and (3) (Ga/III is 0.6 and 0.8, respectively) $CuGa_2$ is present and no Cu–In intermetallic is detected. This observation indicates that the formation of $CuGa_2$ is favored. In diffractogram (2) additional peaks corresponding to a ternary $Cu(Ga,In)_2$ alloy are detected. In both diffractograms (2) and (3) the metallic In diffraction peaks are more intense than in diffractogram (1). This observation indicates that in environments with higher Ga content the In prefers to remain in metallic form, rather than to alloy with Cu or to substitute Ga in $CuGa_2$. Previously we observed $CuGa_2$ when codepositing Cu–Ga from ChCl : U[5] and $CuIn/Cu_2In$ when plating Cu and In from ChCl : U.[6] Zank and co-workers observed $CuGa_2$ and no In alloy in a precursor with Ga/III = 0.5 when coelectrodepositing In and Ga from an aqueous electroplating bath onto Cu substrates.[4]

To sum up, in this section we demonstrated that the Ga/III ratio of Mo/Cu/In–Ga stacks can be controlled, with a set of two regimes where one follows a clear linear trend, in a large composition range from $0.1 \leq$ Ga/III ≤ 0.9.

3. Solar cell characterization

In order to test the performance of solar cells grown *via* the deposition route in study, Mo/Cu/In–Ga precursors were plated with Cu/(In + Ga) = 0.7 and an experimentally determined Ga/III = 0.4. These precursors were thermally annealed in a three-stage process, which aims at diminishing Ga accumulation at the back of the absorber layer, typically observed in one step selenizations.[3] Fig. 6(a) depicts the J–V curve of the finished device, which achieved an efficiency of 7.9%, with a total surface area of 0.485 cm^2, with FF = 56%, J_{sc} = 26.6 mA cm^{-2} and V_{oc} = 520 mV. The latter figure is higher than V_{oc} for the CIS record cell (491 mV),[16] indicating that Ga was incorporated into the photoactive semiconductor lattice. The reported V_{oc} is high, compared to other CIGS solar cells grown by electrodeposition processes. Bhattacharya[17] and Ribeaucourt[3] reported 427 mV and 456 mV for solar cells with efficiencies of 10.9% and 9.3%, respectively. However, J_{sc} obtained in this work is much lower, with the referred authors obtaining 38.6 mA cm^2 and 32.8 mA cm^2, respectively. Such findings can be explained by the EQE measurement (Fig. 6(b)), where high losses for λ > 700 nm are observed and a maximum of 82% is obtained. Further EQE measurements under reverse bias did not influence the shape of the curve at higher wavelengths (λ > 800 nm). This observation indicates that the collection is not improved when applying a reverse bias, which can be either due to a small space charge region or a low diffusion length. Another factor hindering current generation is the low thickness of the absorber (approximately 1 μm). Z. Jehl *et al.* observed a pronounced decrease of approximately 30% in the J_{sc} by thinning CIGS absorber layers from 2.5 μm to 500 nm *via* chemical etching, whilst the V_{oc} remained nearly constant.[18] The authors attributed this observation to absorption losses,

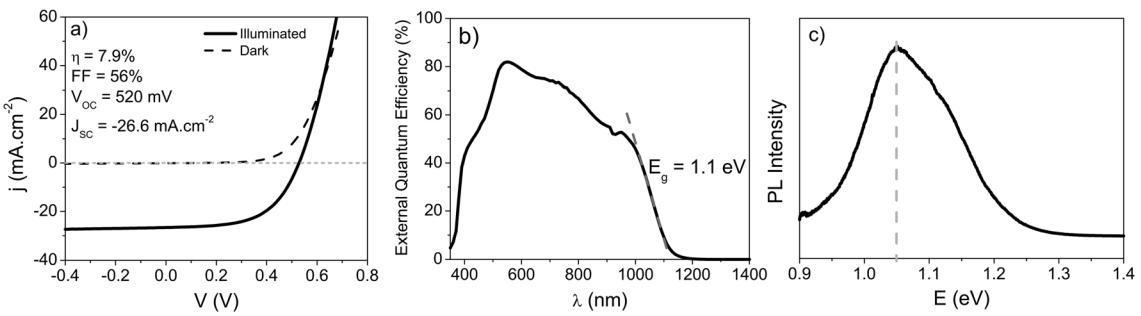

Fig. 6 (a) J–V curve of a complete Mo/CIGS/CdS/I–ZnO/Al : Zno/Ni/Al solar cell and (b) external quantum efficiency measurement. In plot (c) the room temperature PL spectrum of the matching absorber is depicted. The CIGS absorber and the finished device originated from a Mo/Cu/In–Ga precursor with Cu/(In + Ga) = 0.7 and a Ga/III ratio of 0.4 as measured by ICP-AES.

increased reflectivity of the layers and higher recombination at the back contact.

From the EQE measurement a band gap of 1.1 eV was extrapolated. This value confirms that there is a photoactive Cu(In,Ga)Se_2 layer, since it is above the band gap of $CuInSe_2$ (E_g = 1.0 eV).[19] However, a band gap of 1.1 eV corresponds to a Ga content of 10%, below the value of 40% of the precursor. This difference is originated by Ga accumulation at the back of the absorber layer during the selenization. This segregation effect can also negatively influence the J_{sc} of the device. By integration of the EQE measurement a J_{sc} of 26.8 mA cm^{-2} is obtained, in good agreement with result from the *J–V* analysis. Fig. 6(c) depicts the room temperature PL spectrum of the corresponding CIGS film and shows a broad asymmetric peak, with a maximum at 1.05 eV, in good agreement with the EQE extrapolation. The shoulder on the high-energy side of the peak indicates that there are CIGS phases with higher Ga content, originated by the Ga segregation to the back of absorber layer.

To sum up, it was shown that the growth route used in the study is adequate to synthesize Cu–In–Ga metal precursors which can be processed into efficient solar cells. EQE and PL studies showed that the absorber layer was too thin and that Ga segregation occurred. The latter issue can be corrected by optimizing the annealing procedure. Moreover, to improve device performance the Cu/(In + Ga) ratio of the precursor has to be adjusted to approximately 0.9.[20]

Experimental

Experiments related to synthesis and electrochemistry were performed in a glovebox (MBraun Unilab) in an inert nitrogen atmosphere. Water and oxygen contents inside the glovebox were lower than 1 ppm at all times. The ionic liquid was synthesized by mixing Choline chloride (Sigma-Aldrich 99.8%) and Urea (Sigma-Aldrich 99.5%) in a 1 : 2 molar ratio. Further details of the preparation of the liquid can be found elsewhere.[5] Anhydrous $GaCl_3$ (Alfa Aesar 99.999%) and $InCl_3$ (Alfa Aesar 99.999%) were used as received. A three electrode cell was used to conduct the electrochemical experiments. The counter and reference electrodes were a platinum foil and a silver wire, respectively. Massive molybdenum and copper disks were used as working electrodes for cyclic voltammetry (CV) experiments in a rotating disk configuration. By using a rotating disk electrode (RDE) we guarantee time independent diffusion control, improved lateral homogeneity of the deposits and higher deposition rates. An Ecochemie μAutolab type III potentiostat was used as a power source. Indium and gallium were coelectrodeposited onto Mo substrates or onto Mo/Cu thin films, both with a surface area of approximately 4 cm^2. The Cu was electrodeposited from a ChCl : U–$CuCl_2$ electrolyte, which contained an organic additive to allow the deposition of smooth and lustrous copper films. The Mo substrates were subjected to a three step cleaning process: first the substrate was etched for 5 minutes in 30 vol% NH_4OH (Carl Roth 99.99%) and then ultrasonically cleaned in deionized water (18.2 MΩ cm) and absolute ethanol (Fisher Scientific 99.99%) for 5 minutes.

As deposited metal precursors containing Cu, In and Ga were subjected to a three-step annealing procedure, based on the work of Kim *et al.*[11] The first step consisted of a first selenization at 400 °C. In the second step, the film is annealed at 550 °C under N_2 flow and in the last step the absorber is subjected to a second selenization at 550 °C to rechalcogenize the CIGS layer. After annealing the resulting thin films were etched in a 5 wt% KCN solution for 30 seconds to remove $Cu_{2-x}Se$ phases. Samples were then processed in order to obtain solar cells with the following structure: Mo/CIGS/CdS/i-ZnO/Al : ZnO/Ni/Al. Grazing incidence X-ray diffraction (XRD) measurements were performed on a Brüker Discover D8, using Cu K_α radiation with λ = 1.5418 Å and an incidence angle of 3°. Scanning Electron Microscopy (SEM) was performed on a Hitachi SU-70 microscope coupled to an Oxford Instruments INCA X-MAX spectrometer for Energy Dispersive X-ray Spectroscopy (EDX) analysis. Inductively Coupled Plasma Atomic Emission Spectroscopy (ICP-AES) was performed on a Horiba Jobin Yvon Activa M. Prior to the ICP-AES analysis, the samples were dissolved in a 3 : 1 (vol.) mixture of HCl : HNO_3 (conc.). Room temperature photoluminescence (PL) measurements were performed using as an excitation source the 514.5 nm Ar ion laser line. The PL photons were collected and then dispersed in a 0.3 m spectrometer. An InGaAs detector array was used. The CIGS absorbers were measured by PL as grown and not subjected to any treatment prior to the measurement. Current–Voltage (*I–V*) and External Quantum Efficiency (EQE) measurements were performed at T = 25 °C, under AM1.5 illumination. The latter characterization method consists of measuring the short circuit current (J_{sc}) of the solar cell as a function of the incident light wavelength. The measurement output represents the number of collected electrons (at the load) per incident photon.

Conclusion

In this work a new method was introduced, allowing the full control of the Ga content ($0.1 \leq$ Ga/III ≤ 0.9) of Cu–In–Ga metal precursors for CIGS solar cells. The Ga/III control mechanism depends solely on the flux of material to the working electrode. The wide potential region where constant mass fluxes are ensured makes the ED of indium and gallium from ChCl : U an interesting process for large scale industrial ED applications, as high voltage drops across the surface of the substrate can be tolerated. Furthermore, no additives are required. Such fine control of the Ga content was not possible before by any other Cu–In–Ga electroplating growth process. The electrochemical behavior of the ChCl : U–$GaCl_3$–$InCl_3$ system on Mo and Cu electrodes was studied and was based on the superposition of the ChCl : U–$GaCl_3$ and ChCl : U–$InCl_3$ systems. Codeposition of In and Ga on Mo substrates results in the growth of Ga droplets with In crystallites on the surface. No alloying phenomenon was observed, as expected from the In–Ga binary phase diagram. When codepositing In–Ga on Cu it was observed that the morphology, crystalline structure and element distribution depended on the Ga content of the deposit. Regarding the morphology, for low Ga contents, the growth of In agglomerates on a nearly

 This journal is © the Owner Societies 2014

covered Cu–Ga–In bottom layer was observed, while for increasingly higher Ga contents, a Cu–Ga underlayer became increasingly exposed, with pure In islands on its surface. The formation of CuIn was only observed for low Ga contents, with $CuGa_2$ being preferred in intermediate and Ga-rich environments. The formation of Cu–Ga–In alloys was also observed.

Metal stacks of Mo/Cu/In–Ga were successfully selenized to form the chalcopyrite CIGS. Solar cells based on this absorber achieved a maximum 7.9% efficiency, with a high V_{oc} above 500 mV. A low J_{sc} was obtained due to a low absorber thickness, which caused deficient carrier generation as shown from EQE measurements. Room temperature PL presented a broad asymmetric peak, indicating that there was Ga segregation towards the Mo back contact. Solar cell performances can be further increased by adjusting the Cu content, thickness of the precursors and by optimizing the annealing routines.

Acknowledgements

J.M. and D.R. thank the Fonds National de la Recherche du Luxembourg (FNR) for AFR PhD grants no. 1080203 and 785084, respectively. M.S. thanks the FNR for a CORE Junior Track Project (C11/MS/1211521) and P.D. for the ATTRACT Fellowship Grant (07/06). The authors thank Maxime Thevenin (University of Luxembourg) for the Mo, CdS and i-ZnO/Al : ZnO depositions and Michael Kirsch (Helmholtz Zentrum Berlin) for Ni/Al grid deposition. The CRP Gabriel Lippmann is acknowledged for the use of XRD and SEM/EDX equipment.

References

1 P. Jackson, D. Hariskos, E. Lotter, S. Paetel, R. Wuerz, R. Menner, W. Wischmann and M. Powalla, *Prog. Photovolt. Res. Appl.*, 2011, **19**, 894–897.
2 V. S. Saji, I.-H. Choi and C.-W. Lee, *Sol. Energy Mater.*, 2011, **85**, 2666–2678.
3 L. Ribeaucourt, E. Chassaing, G. Savidand and D. Lincot, *Thin Solid Films*, 2011, **519**, 7241–7244.
4 J. Zank, M. Mehlin and H. P. Fritz, *Thin Solid Films*, 1996, **286**, 259–263.
5 M. Steichen, M. Thommassey, S. Siebentritt and P. J. Dale, *Phys. Chem. Chem. Phys.*, 2011, **13**, 4292–4302.
6 J. C. Malaquias, M. Steichen, M. Thomassey and P. J. Dale, *Electrochim. Acta*, 2013, **103**, 15–22.
7 A. Duchatelet, G. Savidand, R. N. Vannier, E. Chassaing and D. Lincot, *J. Renewable Sustainable Energy*, 2013, **5**, 011203.
8 A. Duchatelet, T. Sidali, N. Loones, G. Savidand, E. Chassaing and L. Lincot, *Sol. Energy Mater. Sol. Cells*, 2013, **119**, 241–245.
9 A. J. Bard and L. R. Faulkner, in *Electrochemical Methods Fundamentals and Applications*, ed. D. Harris and E. Swain, John Wiley & Sons, Inc., New York, 2nd edn., 2001, p. 98, 337–339.
10 T. J. Anderson, *J. Phase Equilib.*, 1991, **12**, 64–72.
11 K. Kim, G. M. Hanket, T. Huynh and W. N. Shafarman, *J. Appl. Phys.*, 2012, **111**, 083710.
12 G. M. Hanket, W. N. Shafarman, R. W. Birkmire, *Conference Record of the 2006 IEEE 4th World Conference on Photovoltaic Energy Conversion*, 2006, **1**, 560–563.
13 M. Purwins, R. Enderle, M. Schmid, P. Berwian, G. Müller, F. Hergert, S. Jost and R. Hock, *Thin Solid Films*, 2007, **515**, 5895–5898.
14 A. Brummer, V. Honkimäki, P. Berwian, V. Probst, J. Palm and R. Hock, *Thin Solid Films*, 2003, **437**, 297–307.
15 G. S. Chen, J. C. Yang, Y. C. Chan, L. C. Yang and W. Huang, *Sol. Energy Mater. Sol. Cells*, 2009, **93**, 1351–1355.
16 J. A. M. AbuShama, S. Johnston, T. Moriarty, G. Teeter, K. Ramanathan and R. Noufi, *Prog. Photovolt. Res. Appl.*, 2004, **12**, 39–45.
17 R. N. Bhattacharya, M.-K. Oh and Y. Kim, *Sol. Energy Mater. Sol. Cells*, 2012, **98**, 198–202.
18 Z. Jehl, N. Naghavi, L. Lombez, I. Gerard, M. Bouttermy, P. Tran-Van, A. Etcheberry, G. Voorwinden, B. Dimmler, W. Wischmann, M. Powalla, J. F. Guillemoles and D. Lincot, *Thin Solid Films*, 2011, **519**, 7212–7215.
19 T. Dullweber, G. Hanna, W. Shams-Kolahi, A. Schwartzlander, M. A. Contreras, R. Noufi and H. W. Schock, *Thin Solid Films*, 2000, **361–362**, 478–481.
20 M. Kemell, M. Ritala and M. Leskelä, *Crit. Rev. Solid State Mater. Sci.*, 2005, **30**, 1–31.